GEM-TN-94-607

A Simple Technique for Measuring Axial Displacement in Stretched-Wire Alignment Systems

J. Paradiso
Draper Laboratory

May 1994

Abstract

A method is described for determining axial displacement along a stretched wire by driving both ends of a resistive wire as a bi-directional voltage divider and measuring the local signal balance with a capacitive pickup. Such a system has been constructed, and test results are presented, along with the details of the electronics and apparatus, plus a description of the intended application of this technology in the GEM muon system. The factors limiting the measurement resolution are discussed, and suggestions are given to improve performance. In addition, the wire readout electronics are shown to be able to accurately monitor the mechanical resonance in a stretched wire, enabling the wire sag to be determined.

A Simple Technique for Measuring Axial Displacement in Stretched-Wire Alignment Systems

-- J. Paradiso , May '94

1) GEM Motivation

At the conclusion of the GEM project, the most favored alignment technique for the GEM muon barrel[1] was the hybrid "axial/projective" concept[2], shown in simplified form in Figs. 1 and 2. Under this approach, 3-point optical projective monitors[3] are used to measure the sagitta error between the three superlayers at the barrel edges ($\theta = 90°$ and 30°), and a multipoint axial monitor (i.e. stretched wires) is used in each superlayer to define straight lines across the separate muon chamber packages stacked along the z direction. The axial and projective monitors are both referenced to precision, stress-free, composite transfer plates ("Alignment Reference Bars" in Fig. 2), which provide a common interface between the interlayer and axial alignment systems.

Granted, the mechanical stability of these transfer plates is a crucial issue (they were under design at GEM's conclusion). An unmodelled bend across the plates could be compensated in various manners, however, the most obvious being the introduction of additional 3-point interlayer monitors between the triad already depicted at each end of the tower, providing more points across the plates for interpolation.

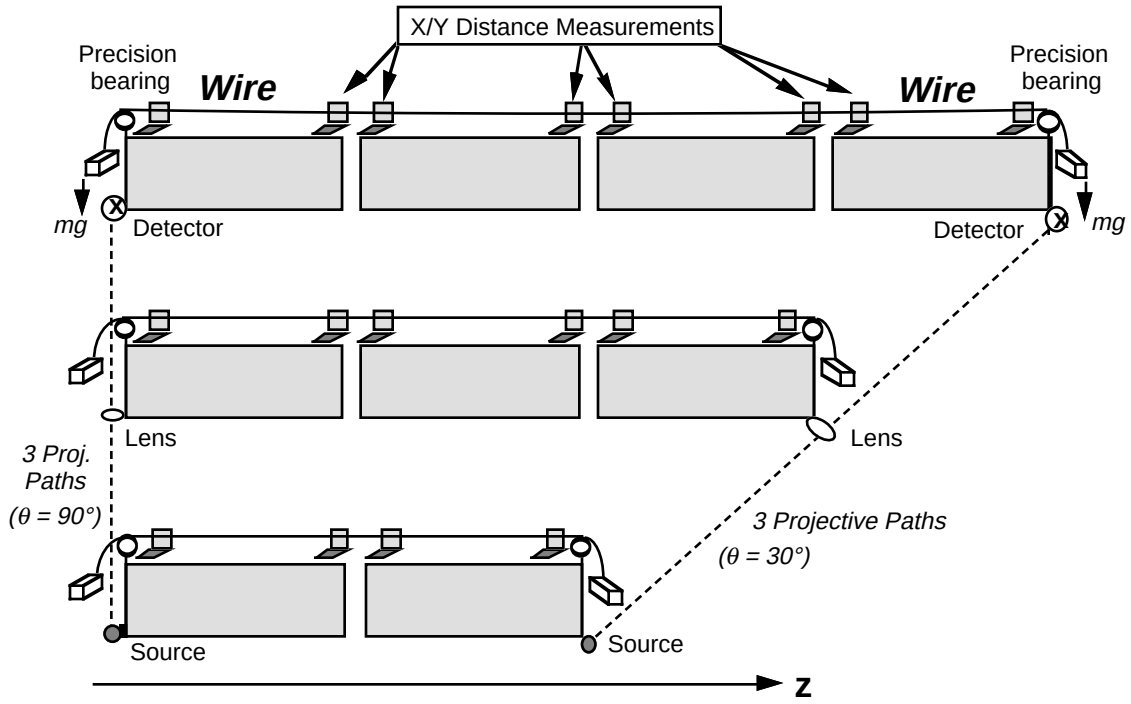

Figure 1: Basic concept of axial/projective alignment

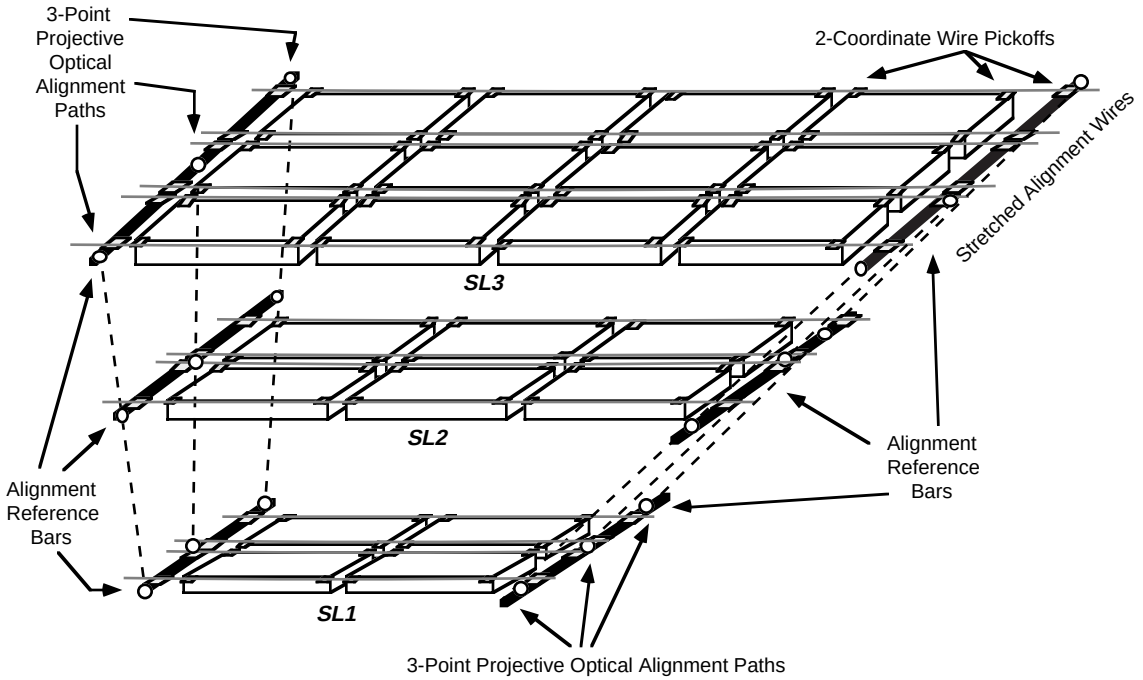

Figure 2: Axial/Projective alignment as applied to GEM Barrel Module

Several direct advantages of adopting this strategy (i.e. increased acceptance by butting chamber ends together in z, ability to measure of chamber sag, simpler implementation) are discussed in Refs. [4,5,6].

The gist of this philosophy is the application of two alignment systems; one "sub-local", that relates many small detector packages (i.e. the GEM cathode strip chambers) together to form large fiducial areas, plus another (potentially more complicated/expensive) alignment system working at a higher level of abstraction in order to measure the displacement between these fiducial aggregates. Provided that the two systems function to the required precision and mechanical alignment transfers are kept sufficiently minimal, strict overall alignment requirements can be maintained (in GEM, the anticipated performance of the hybrid axial/projective system was simulated[6,7] to ensure that it was able to meet our 25 μm sagitta alignment requirement).

This philosophy delivers an added benefit in simplifying the systems needed for global alignment (i.e. determining the position of the detector components relative to the interaction point) and streamlining the survey/installation procedure. As seen in Fig. 2, the rϕ displacement of all chambers in a barrel tower superlayer can be determined by measuring fiducials on the alignment reference bars at each end. The axial alignment system (i.e. stretched wires) transfers the displacements of all chambers spanning its paths into the reference bars. By surveying the ends of the alignment wires (i.e. the

reference bars), the positions of all chambers measured by the wires are determined; there is no need to survey each and every chamber in a barrel tower, a daunting prospect for any survey crew[8]. In addition, sighting alignment bars at the barrel tower edges ($\theta = 30°$ and 90°) present the best installation survey opportunities, since a stage set up outside the detector can observe this region easily (as opposed to the difficulty in obtaining a line-of-sight to points on chambers placed inside the barrel, obscured by the mechanical structure).

A similar advantage follows after the detector is installed. At GEM, the only gaps in the magnet cryostat through which a sighting was possible for global alignment occurred at the 30°\90° barrel edges. Under the scheme of Fig. 2, a line-of-sight reference to the alignment bars may be extracted relatively easily through these gaps, allowing the global alignment to be monitored.

By using interpolative projective alignment[9], the mechanical positioning of chamber packages is considerably relaxed; chamber displacements of up to several millimeters and rotations reaching a few milliradians can be compensated by the alignment measurements. Specifically, the GEM analysis indicated that chamber placement in various coordinates (including the axial [z] direction) should be adjusted to within 1.5 to 3 mm of nominal[1,10]. If one employs stretched wire monitors, as in Figs. 1 & 2, the mini-strip readout scheme can measure the bending (x) misalignment to well under 10 μm, and determine the radial (y) coordinates with better than 100 μm, as demonstrated in Ref. [5]; this is certainly more than adequate for filling the mm-level installation positioning requirement when the wire system is used to transfer survey measurements across the barrel, as discussed above.

The mini-strip readout, however, as defined in Refs. [5,6], lacks any provision for measuring the axial [z] position along the wire. An inexpensive augmentation of the wire readout to provide a coarse, mm-level axial displacement measurement would be of considerable benefit, both in streamlining the initial survey and in monitoring the detector alignment after installation (granted, a mm-level detector disturbance would be fairly extreme, but may be possible after an access, for example). This document describes a simple system to realize this goal; i.e. measure the axial displacement along a stretched wire.

2) Axial Position Measurement

Figure 3 shows a block diagram of the proposed axial measurement system. The essential principle revolves around the application of a resistive wire. If a driving AC voltage is introduced at one end, and the opposite end is grounded, an ideal wire acts as a voltage divider. If one moves a high-impedance voltmeter probe down the wire, the recorded voltage will be proportional to the fractional displacement of the probe tip from the grounded end (much as in measuring at the wiper of a potentiometer). The capacitive pickup in Fig. 3 performs the function of the voltmeter probe (or potentiometer wiper); i.e. it provides a very high impedance (typically, C < 1 pf) noncontact (r > 1 cm) tap into the local wire signal.

Although the capacitive pickoff may be fashioned from various shapes, a simple conducting ring has been chosen for the tests performed here. The ring has several advantages as an axial sensor; i.e. it presents a large area for coupling into the wire signal, it can be readily shielded such that it is sensitive to a small region of the wire at fixed axial distance, and it is less sensitive to displacement of the wire away from its center.

A synchronous detection scheme is employed to measure the signal coupled from the wire, as was used with the mini-strip readout system[6]. As depicted in Fig. 3, an

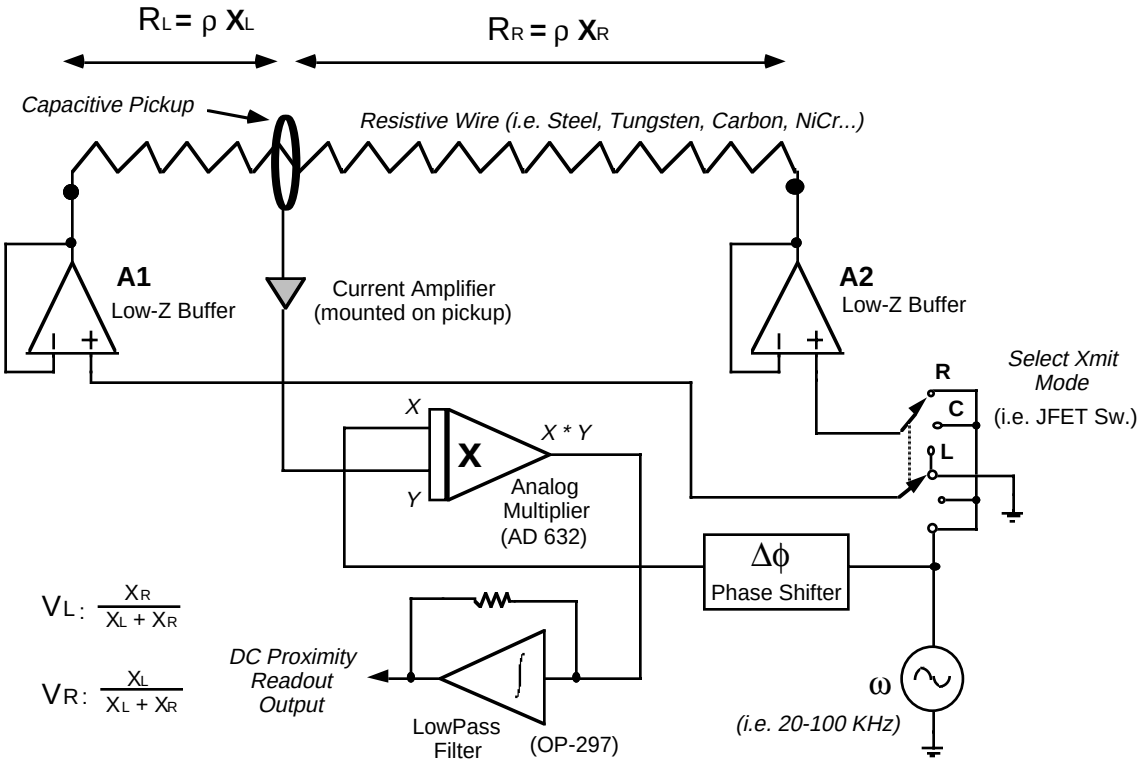

Figure 3: Axial Measurement Technique

analog multiplier demodulates the pickup signal with the same waveform applied to the wire; the detected signal then has components at DC and twice the transmitted frequency (ω). A low-pass filter selects the DC component, simultaneously filtering out most out-of-band interference, thereby providing a detection with very low extraneous noise.

This signal is ideally proportional to the driving voltage, weighted by the fractional distance along the wire from the location of the pickup to the grounded end. Referring to Fig. 3, and assuming that we are measuring with the oscillator driving the right side of the wire and left side grounded (the switch set to "R"), this can be expressed:

1) $$V_R = \alpha_g V_0 \gamma_c \frac{\rho_L x_L}{\rho_L x_L + \rho_R x_R}$$

where ρ is the resistance per unit length of the wire (ρ_L, ρ_R are averaged over left and right segments), V_0 is the oscillator drive voltage, γ_c is the efficiency of the capacitive coupling between wire and pickup, α_g describes the gain of the readout circuit, and $x_{L,R}$ are the distances of the pickup from left and right wire ends. An analogous situation occurs when the switch is flipped to "L", and we are driving the left side of the wire:

2) $$V_L = \alpha_g V_0 \gamma_c \frac{\rho_R x_R}{\rho_L x_L + \rho_R x_R}$$

Since (again, in the ideal case; the realistic situation will be dealt with later) V_0 is identical at each side (as seen in Fig. 3, low-impedance voltage followers buffer each end of the wire), α_g doesn't change (we use the same readout electronics when driving either end of the wire), γ_c is identical (we measure with the same pickup sensor), and ρ is uniform across the wire (i.e. $\rho_L = \rho_R$), the constant terms cancel out of the voltage ratio:

3) $$\frac{V_L}{V_R} = \frac{x_R}{x_L}$$

This provides a clean estimate of the relative distance across the wire, however it goes nonlinear as one approaches either end. A better formulation is provided by:

4) $$\beta \equiv \frac{V_L - V_R}{V_L + V_R} = \frac{x_R - x_L}{x_R + x_L}$$

which is zero at the midpoint of the wire, and ramps linearly to ±1 at each respective end.

This technique is similar to that of charge division readout used in drift chambers[11]. Here, however, we can exploit the synchronous detection system outlined in

Fig. 3 (plus integrate the signals for a long period), and thus achieve a much higher signal-to-noise.

The same wire can be used for the mini-strip readout of transverse and radial coordinates[5]; to obtain maximum signal for this measurement, both ends of the wire would be driven together in phase (with Xmit mode switch in "C" position; Fig. 3). The Xmit mode switch would be toggled electronically by the data acquisition computer in order to select the appropriate measurement.

Since the front-end amplifier is wired as a current-input stage, the detected voltage V_d is proportional to the current coupled into the pickup (i.e. the drive voltage V_0 scaled by the drive frequency ω and the net wire-to-pickup capacitance C_{pw}). Since the C_{pw} is small (i.e. <1 pf typically), and the input amplifier impedance is very low, this circuit is a hard differentiator, hence V_d phase-shifted by 90° (not accounting for potential rolloff effects at the input amplifiers); the phase shifter block ($\Delta\phi$) in Fig. 3 brings the receive signal back into phase with the reference for coherent demodulation. This can be summarized:

5) $$V_d \propto V_0(j\omega C)$$

Needless to say, reality is seldom ideal, and here it can intrude on our measurements via several different routes. The dynamic range required for this measurement can be quite wide, depending on the application. At GEM, our longest wire would have been stretched across 15 meters. Requiring a 1.5 mm axial error along that length entails a dynamic range of 1 part in 10^4. By comparison, the seemingly more stringent sagitta alignment measurement requirement[5,6] of 10 μm (transverse to the wire) over a range of 1 cm requires only 1 part in 10^3. Most errors affecting the axial measurement hide in the constant factors multiplying Eqs. 1 & 2, and are outlined below.

The driving sinusoid is fanned out to voltage followers at each end of the wire. As these voltages are reasonably modest (tests found 30 V p-p to be much more than adequate), the frequencies fairly low (20-100 kHz), and the wire impedance to be significant (assumed > 100Ω for most cases; see below), this circuitry isn't too critical, and can be realized around a standard OP-AMP (although a high current device will be needed for resistances around 100Ω, this is relaxed at higher resistances). The output impedance of the buffer amplifier must be low and constant (suggesting a feedback amplifier running well away from its voltage\frequency\current limits), and the connection onto the stretched wire must be very secure and stable.

As the resistance of the wire increases, the demands on these buffer amplifiers (and the connections onto the wire) are accordingly loosened. At a certain point, however, capacitive coupling can produce voltage drops along the wire, and affect the measurement. As a rule of thumb, $R_T = \rho L << (\omega C)^{-1}$; i.e. the net resistance of the wire should be well below the reactance provided by capacitive coupling. Assuming that C is under 100 pf (reasonable for a thin wire away from close proximity to conducting surfaces) and f = 50 kHz, R_T should be kept well below 30KΩ. Again, this analysis is strictly approximate; the effect of these losses depends on how the capacitive losses are lumped and on the net precision desired across the wire length.

The resistivity (ρ) of the wire is assumed to be constant in the analysis of Eqs. 1-4, and this is never strictly true; i.e. the resistivity along the wire will depend on factors such as local wire thickness and composition, coating uniformity, etc. If these parameters are stable, the resistance along the wire can be measured and calibrated out (thermal factors not withstanding; see below). Since we are measuring along the entire length of wire, mechanical effects (i.e. nonuniform wire stretch) are integrated across the full span, and influence all measurements directly. The contributions of these errors depend on the particular choice of wire and the quality control applied to its production; by using a superior grade of wire (potentially a composite material), these effects can be minimized.

Thermal gradients will change the local resistivity of the wire; tungsten, with a temperature coefficient[12] of $\Delta\rho/\rho = 0.0045/°C$ is not the best choice from this viewpoint; a wire made from another material (i.e. nichrome, which exhibits[12] $\Delta\rho/\rho = 0.0002/°C$ or a composite with a low temperature coefficient coating) will produce less effect. In order to otherwise operate a precision muon detector, thermal gradients must be kept very low (i.e. at GEM, it was planned[1] to control the temperature within the muon volume to 1° C), hence a wire made from material such as nichrome should exhibit adequate insensitivity.

The electronics gain factor (α_g) is indeed of minimal impact, in that the same set of electronics are used with the pickup to read both ends of the wire. Other effects in the electronics, however, such as bias drift in the DC circuitry (from the multiplier onwards in Fig. 3) can have significant effect, thus the readout electronics must be carefully designed to exhibit excellent DC stability.

The capacitive coupling factor, γ_c, at first glance, presents little problem for a similar reason; the same capacitive pickup (and broadcast frequency ω) is used for reading both left-and-right-driven signals. Upon closer examination, however, difficulties can crop up here as well. In the ideal case, the wire is centered and aligned with the pickup ring axis, producing a coaxial capacitor. This is a classic geometry, with capacitance per unit length (ℓ) given by:

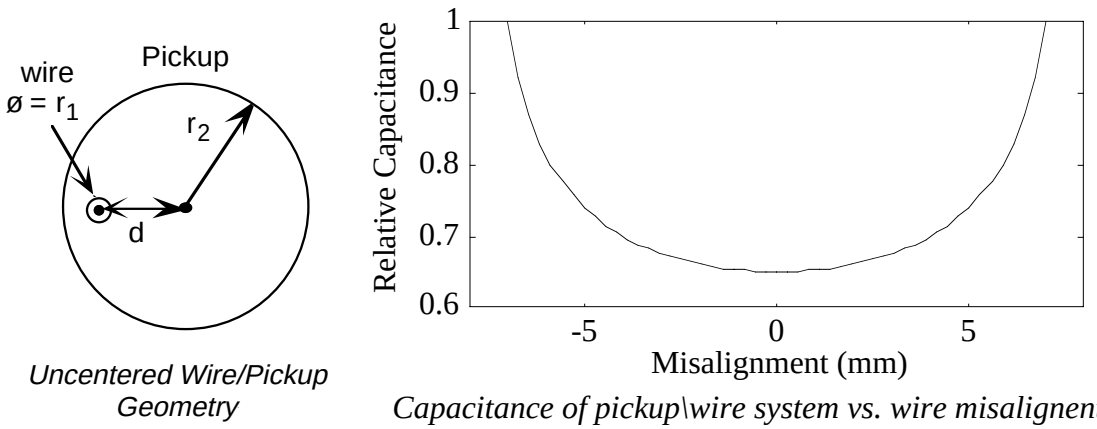

Uncentered Wire/Pickup Geometry

Capacitance of pickup\wire system vs. wire misalignent

Figure 4: Effects of nonconcentricity on the capacitance of the wire/pickup system

6) $$\frac{C_{pw}}{\ell} = -\frac{2\pi\varepsilon_0}{\ln\left(\frac{r_2}{r_1}\right)}$$

where r_2 is the outer (ring) radius and r_1 is the inner (wire) radius.

If the wire shifts significantly away from the center of the coaxial capacitor, the wire-pickup capacitance increases, looking more like a wire-plate coupling as the wire approaches the edge of the ring. Calling the misalignment between the wire and ring centers "d" (see Fig. 4), this is described as[13]:

7) $$\frac{C_{pw}}{\ell} = \frac{2\pi\varepsilon_0}{\cosh^{-1}\left(\frac{\left|d^2 - r_1^2 - r_2^2\right|}{2\, r_1\, r_2}\right)}$$

Fig. 4 also shows a plot of Eq. 7 as a function of d, where we can see that the capacitance is relatively constant when the wire is in the region of the cylinder's center, but increases rapidly as the wire approaches the cylinder wall (the walls are assumed to be placed at r_2 = 8 mm in accordance with the pickup used in our tests). This is yet another advantage of using a ring pickup; the wire-pickup capacitance is relatively unchanged when the wire is displaced within roughly the inner 30% of the ring area.

Because we use the same pickup ring for detecting the signal broadcast from both ends of the wire, at first glance the axial position measurement (β) will be unaffected by changes in C_{pw}. As depicted in Fig. 5, however, a closer look exposes a potential problem. A pickup ring centered on the stretched wire will produce a measurement that is relative to its axial center. This is also true if the ring is translated away from the wire center without rotating its axis, or if the ring is rotated away from axial alignment without

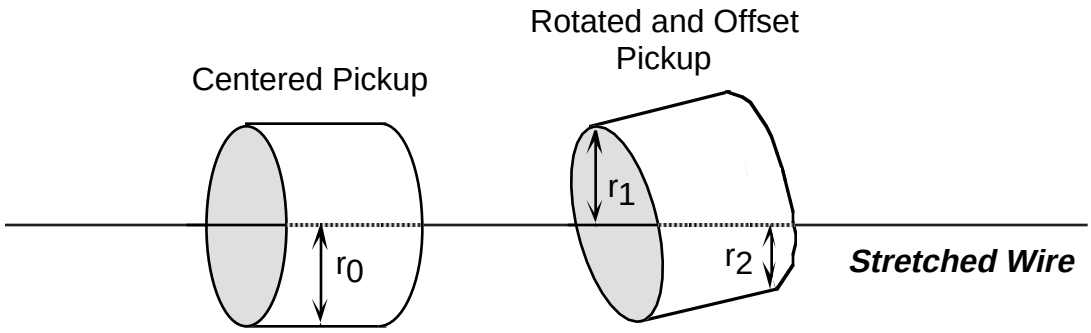

Figure 5: Skew in axial measurement from rotated/offset pickup geometry

translation of its center away from the wire center. If, however, the ring is both translated and rotated (as in Fig. 5), the nonlinear coupling function exhibited in Fig. 5 can skew the axial measurement; i.e. the pickup will couple to the wire more strongly at the shorter radius (r_2 in Fig. 5), causing the effective axial centroid to be displaced in that direction. The practical severity of this effect is limited by a couple of factors. As mentioned above, the cylindrical geometry of the pickup provides a region of flat capacitance near its center (Fig. 4), allowing a modest excursion of wire displacement before this problem becomes significant. In addition, the anticipated amount of off-axis rotation at realistic installations (such as aligning large drift chambers) will generally be quite limited. Nonetheless, depending upon the precision desired, this effect can somewhat constrain the positioning of the wire/ring system such that an approach of the wire to the pickup wall is avoided. The magnitude of effects such as this do not scale with the wire extent (a rotation/translation of each pickup only exerts an effect over the region of wire spanned by the pickup), thus does not present a problem that can grow with the wire length.

Finally, the shielding of the pickup is also a critical issue. The pickup must be constrained to be sensitive to the region of wire upon which it is centered. Coupling to other parts of the wire or to extraneous outside surfaces can produce a large effect on the measurement. This has been successfully dealt with in the experimental setup by abutting insulated grounded rings to each side of the pickup (thereby limiting the axial sensitivity to the local region of wire), and shielding the pickups themselves by mounting them inside of a grounded aluminum box.

In order to better localize the axial centroid, the pickups themselves should be short in the axial direction, but long enough to provide ample coupling into the wire. The 5 mm long rings usid in the tests presented here provided ample signal and good sensitivity, as will be demonstrated in the following sections.

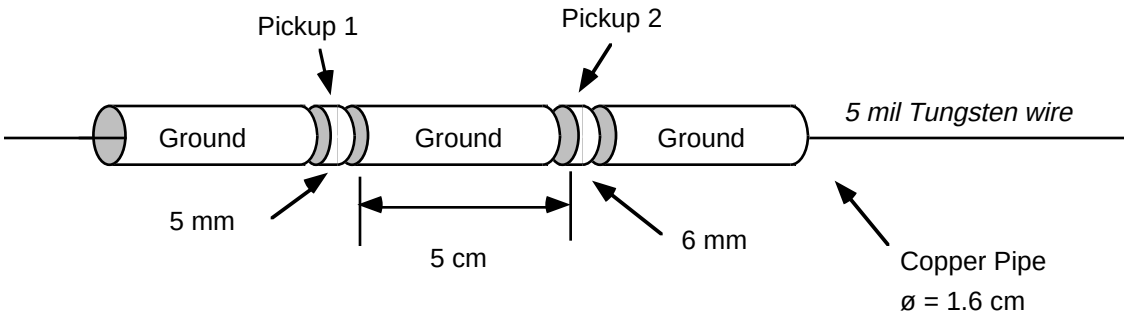

Fig. 6: Mechanical layout of pickup assembly used in tests

3) Experimental Setup

A simple setup along the lines of Fig. 3 was assembled to test the axial readout system. A 5-mil (125 μm) diameter unplated tungsten wire was used, which exhibited a resistivity of $\rho = 40\ \Omega$/meter. The ends were crimp-connected and driven by a Techron 7520 stereo power amplifier (granted, this is excessive, since a pair of power OP-AMPs would be adequate), which constituted A1 and A2 in the figure. The inputs of A1 and A2 were toggled by an electronic DPDT wired around a National Semiconductor LF13201 JFET switch. The frequency reference ω was provided by an HP 3245A Universal Source operating at 50 kHz, and the demodulated output was captured to 5 digits by an HP 3458A Multimeter, which integrated the input samples for 15 seconds. In all tests, data was tabulated by hand; i.e. the micrometer was advanced manually, then the appropriate signals switched into the multimeter and tabulated. This process introduced a delay of over a minute per point, which necessitated a stable frequency reference, thus the HP 3245A. The Techron was generally adjusted to provide a 30 Volt P-P output when driving either end of the wire; this provided very strong signals, and could be run much lower in practice. Data analysis was performed using the MATLAB interpreter[14].

The mechanical pickup assembly is shown in Fig. 6. It is a very simple setup that was fashioned from a standard 1.6 cm inner-diameter copper water pipe with a common pipe-cutter tool. A pair of pickup rings (measuring 5 mm and 6 mm in length) are sandwiched between a triad of 5-cm grounded segments, which serve to constrain the axial acceptance of the pickups, as discussed above. A fiber washer is inserted between each junction to provide insulation, and the entire assembly is held together with 5-minute epoxy. A pair of pickups are built into this unit for a checking the consistency of data and calibration; when performing axial scans, the positions measured at each site should track closely.

Fig. 7 details the signal conditioning electronics that were outlined in Fig. 3. U1 and U2 are configured as current-input operational amplifiers, and are located very close

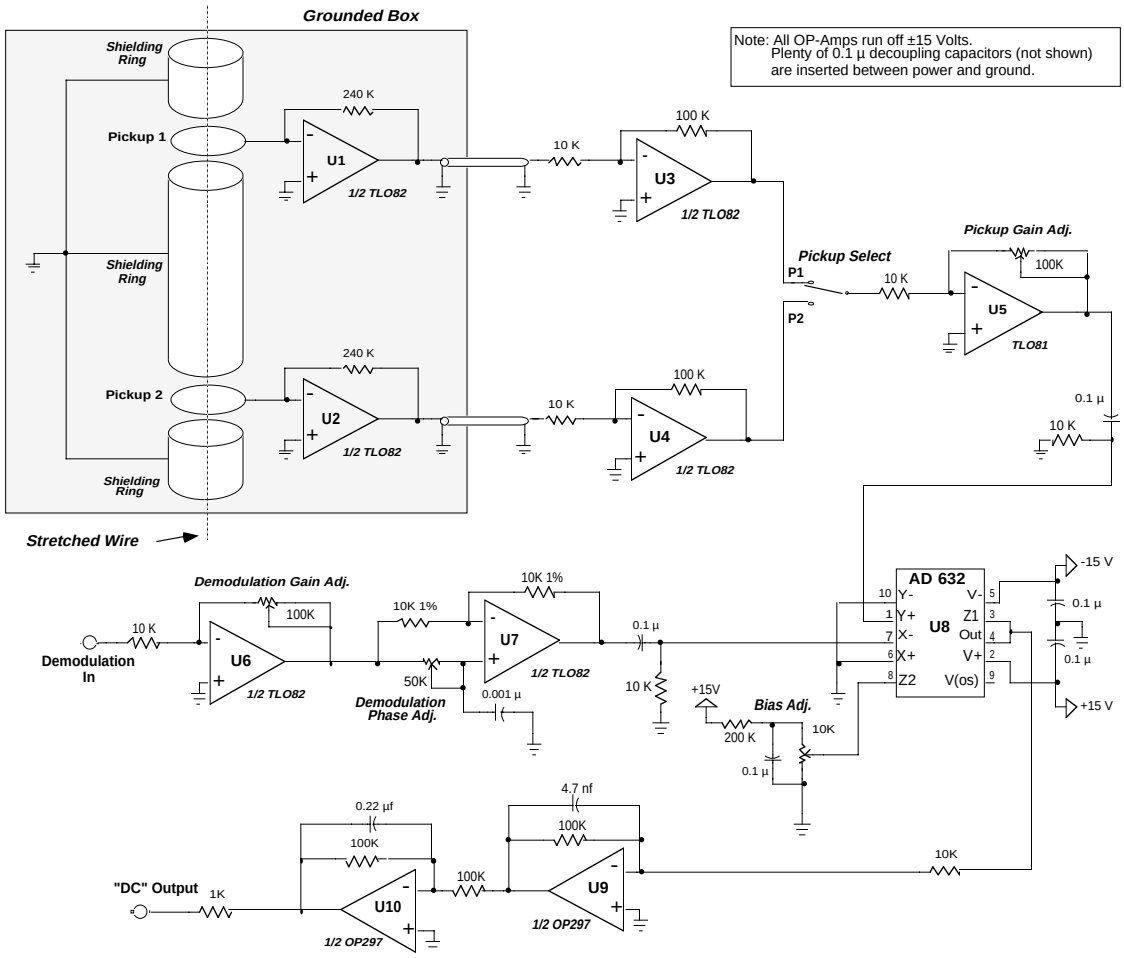

Fig. 7: Schematic showing analog readout electronics for the axial sensor

to the pickup rings, in order to prevent loss or errors from running the raw pickup signals through any length of cable. These rings and amplifiers are shielded in an aluminum chassis, indicated by a gray fill in Fig. 7. The outputs of U1 and U2 are run through several feet of shielded coax to the remainder of the conditioning electronics, all residing on a common circuit card. U3 and U4 provide additional voltage gain, after which either pickup 1 or 2 is selected for readout by the P1/P2 switch. A variable gain stage is provided by U5 before the signal is applied to the analog multiplier U8 for demodulation.

The reference oscillator signal is applied to the demodulation input, where its gain and phase can be adjusted as shown; in these tests, the gain is tweaked at U6 to provide a 5 volt P-P signal at the multiplier input, and the phase is shifted in an all-pass filter (U7) such that the reference signal is in-phase with the amplified pickup signal as applied to the multiplier (as mentioned earlier, the pickup capacitor differentiates the reference

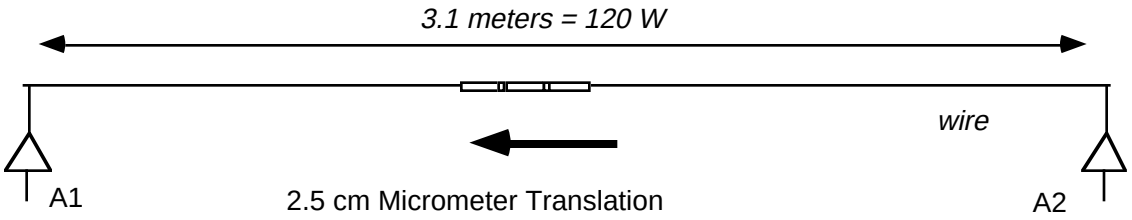

Figure 8: Configuration used for tests of local sensitivity to axial displacement

signal; this, together with the rolloff characteristic of the OP-AMPs, produces a $\Delta\phi$ around 90°). U9 filters the demodulated signal to remove the 2ω component while providing 20 dB of gain. U10 is another low-pass, with cutoff set below 10 Hz to filter the signal additionally and narrow the effective bandwidth to remove extraneous noise from the detected signal. A bias adjustment is provided at the multiplier (U8) in order to enable steady-state DC to be nulled for observing long-term drift.

The selection of components before the multiplier is not highly critical; one basically wants an OP-Amp that performs reasonably at 50-100 kHz, hence TLO-82-class devices have been used. A faster device for U1 and U2 (such as the AD712) will aid performance at the higher frequencies. Because the synchronous demodulation provides a very narrowband response, amplifier noise is not an extreme issue here.

The DC path from the multiplier onward, however, presents a different story, because of the extreme dynamic range that is desired. Here, it is more important to use low-drift, instrumentation-class components and integration capacitors that do not suffer from hysteretic effects; speed is not an issue. As opposed to the inexpensive AD633 multiplier and TLO82 OP-Amps that were used with the mini-strip readout[6], here we use an AD632 precision multiplier and OP297 instrumentation amplifiers for the filter stages. This circuit worked very well in the tests, and displayed little drift.

3) Axial Scan Results

The first set of tests examined the local precision that could be extracted along a short length of long wire. The setup used is shown in Fig. 8. The pickup sensor assembly was placed near to the center of a 3.1 meter long wire span (exhibiting a total resistance of 120 Ω between the crimped ends). The pickups were fixed to a micrometer that was able to precisely translate up to 2.5 cm in all 3 directions, and were aligned "by eye" to be roughly centered and parallel to the wire (owing to the lack of precision in the sensor assembly, the accuracy of this adjustment was limited to a few degrees). The wire was stretched with a 550 gram load. Net capacitance from wire to ground was $\geq$ 30 pf.

The first test using this configuration was a straightforward scan across the 2.5 cm wire segment, sampling the response of both pickup signals to driving the left and right wire ends after each millimeter of displacement. The raw pickup signals are given in Fig. 9 and the corresponding residuals from a linear least-squares fit (drawn over the points in Fig. 8) are plotted in Fig. 10. The left and right columns show data from the left and right pickup rings (labelled "Sensor #1" and "Sensor #2" in the plots), respectively. The top row shows the response when applying the reference oscillator at the left end of the wire, and the bottom row shows the response when applying the reference oscillator at the right end of the wire.

The data appear quite linear, with RMS residuals in the 250-350 μm range. The sensor assembly was placed closer to the left end of the wire; this can be noted from the larger magnitude of the left signals. Some calibration parameters can be noted in the slopes listed with Fig. 9. Sensor #2 appears to be a little more responsive, as expected, since it is roughly a millimeter longer than sensor #1. The left signals are also stronger than the right signals; this is due to a mismatch in the gain of the Techron input channels. Regardless, the form of the residuals for both sensors is very similar, implying that the data will correct further after a ratio is taken.

Indeed, this is what was performed in the data of Fig. 11, where the ratio of left-right difference over sum (β in Eq. 4) is plotted for both pickups (#1 on top, #2 below). This ratio appears to be more linear, and the slopes are now nearly identical for both pickups, implying that the "constant" factors scaling Eqs. 1 & 2 have nearly canceled out, as desired. The residuals from linearity are plotted in Fig. 12, where we see a considerable improvement in accuracy; the β ratios are seen to track the micrometer movement to within σ = 50-70 μm! This is evidence of a very high sensitivity; recall that these measurements were made in the midst of a 3.1 meter length of wire, indicating a dynamic axial measurement range surpassing one part in 10^4.

Figs. 13 & 14 present additional cross-checks that can be made on this system. Fig. 13 shows the deviation of the left plus right signals from their average (as listed) for each sensor (plotted in Fig. 9), after correcting for the imbalance in the driver gains. Ideally, this should be flat, as the wire should function as a perfect voltage divider; indeed, it's flat to better than 1 part in 10^3. The deviations from average are strongly correlated between both pickups (hence they divided out in the ratio), indicating a collective effect such as a drift in the reference oscillator or (more probably) a shift in the mechanics of the system; i.e. displacement of the wire relative to the pickup walls. The wire was stretched across a standard workbench in these tests, and temperature was not controlled, hence mechanical effects at these levels are hardly unexpected.

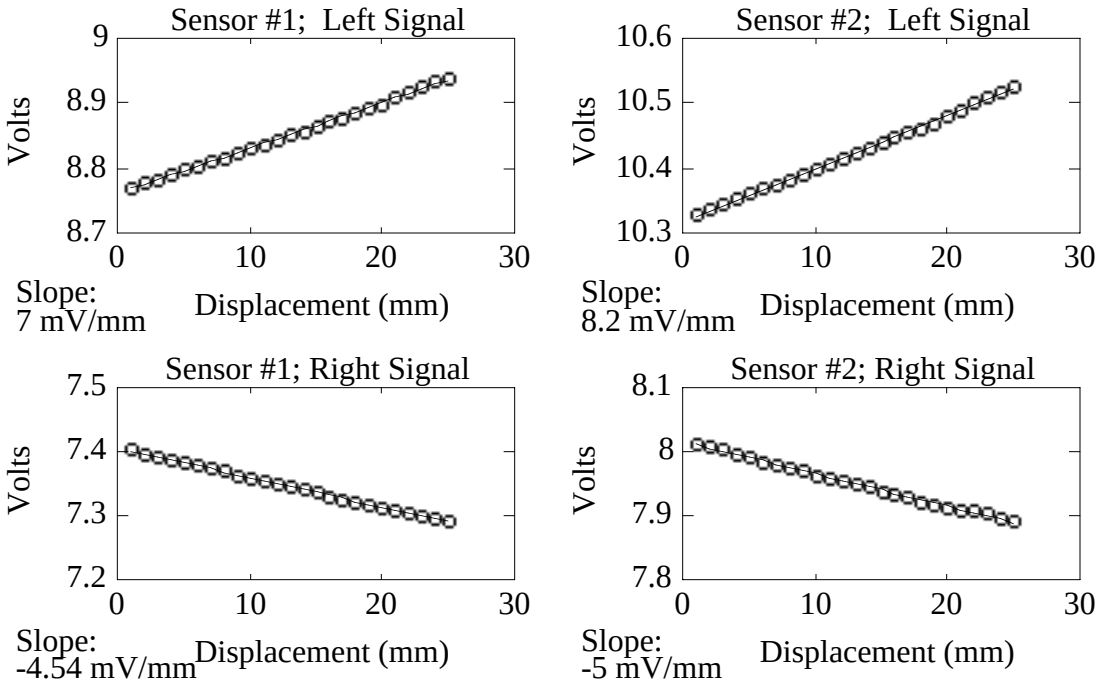

Figure 9: Pickup signals as a function of local axial displacement

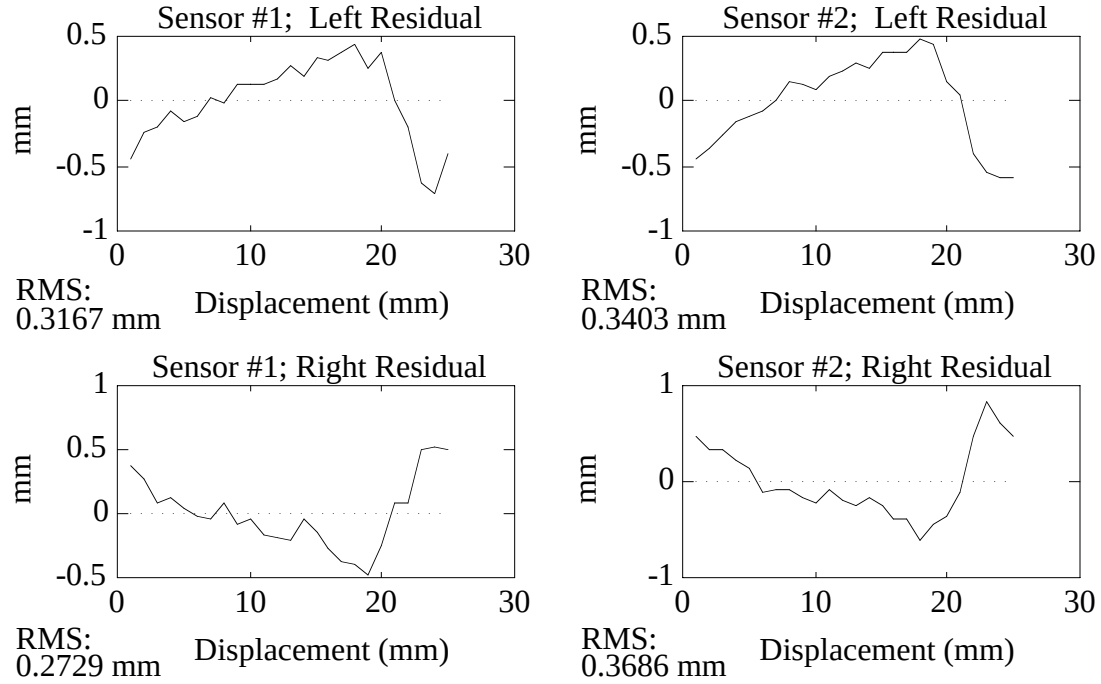

Figure 10: Linear residuals from pickup signals as a function of local axial displacement

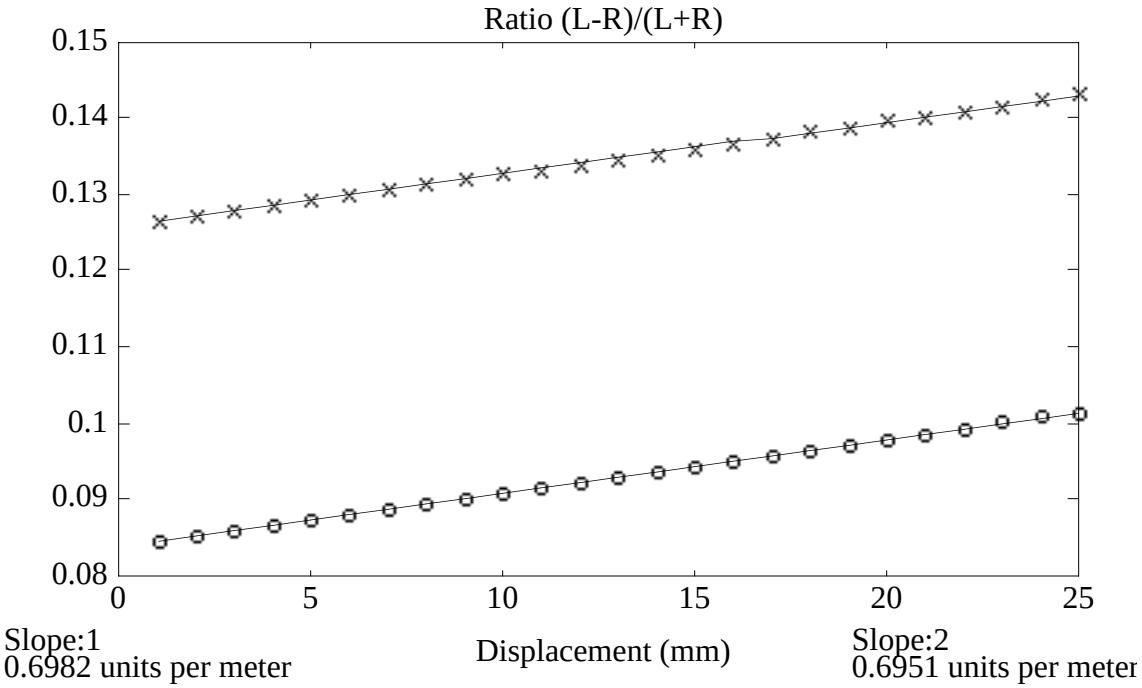

Figure 11: Sum over difference ratio β as a function of local axial displacement

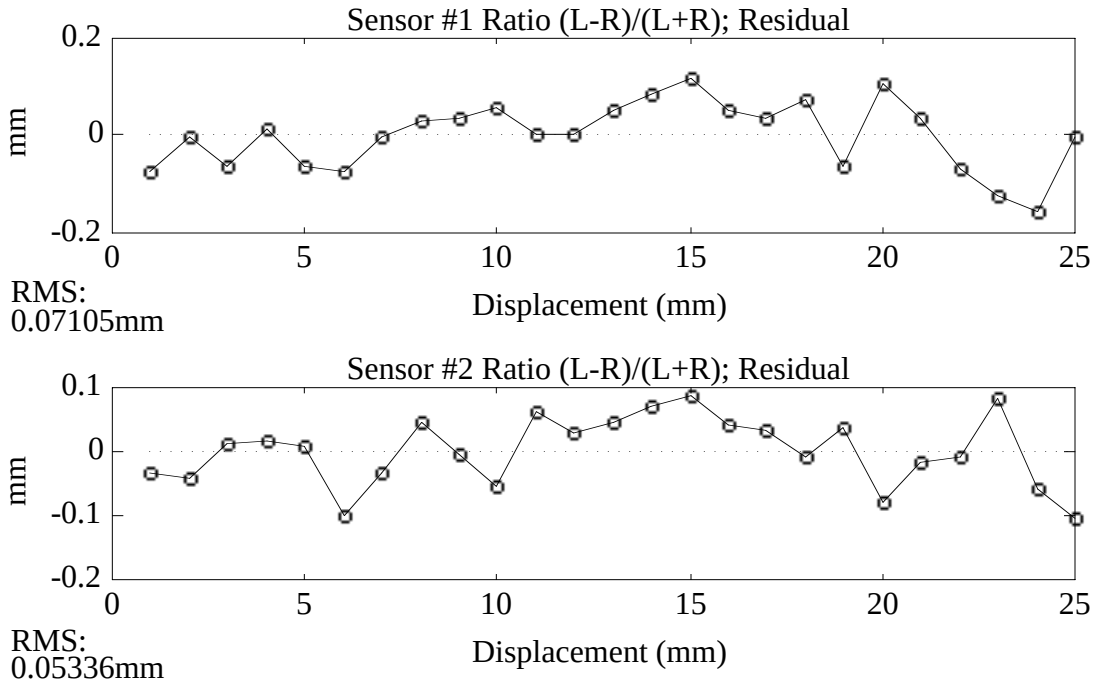

Figure 12: Linear residual of β as a function of local axial displacement

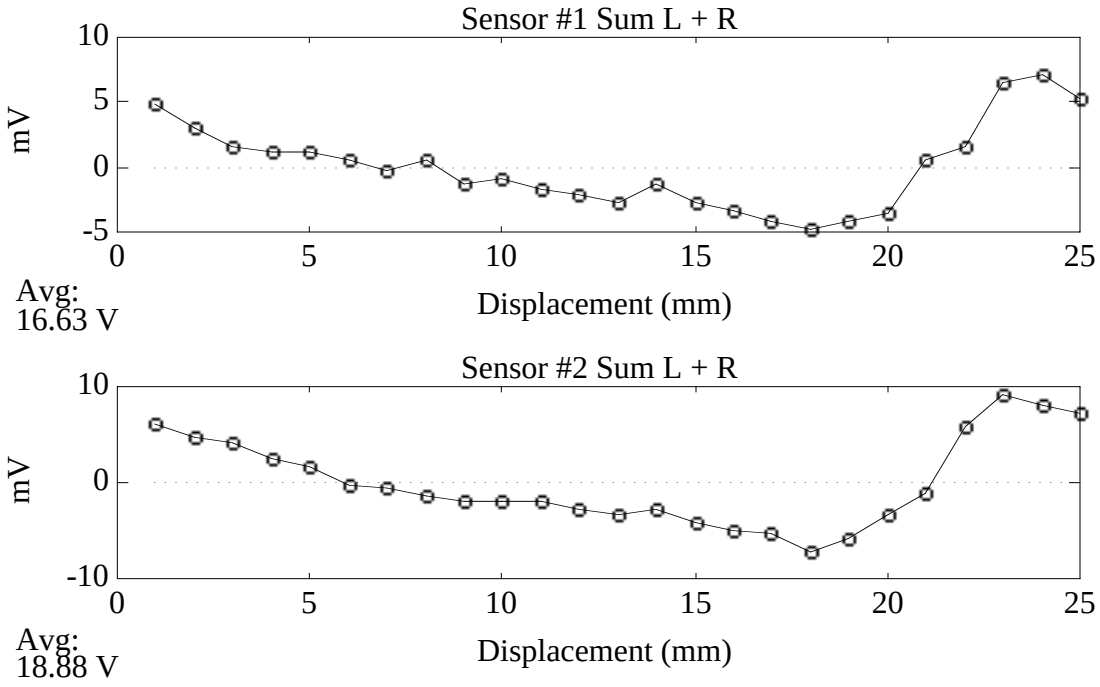

Figure 13: Sum of Left and Right signals from each pickup over local axial displacement

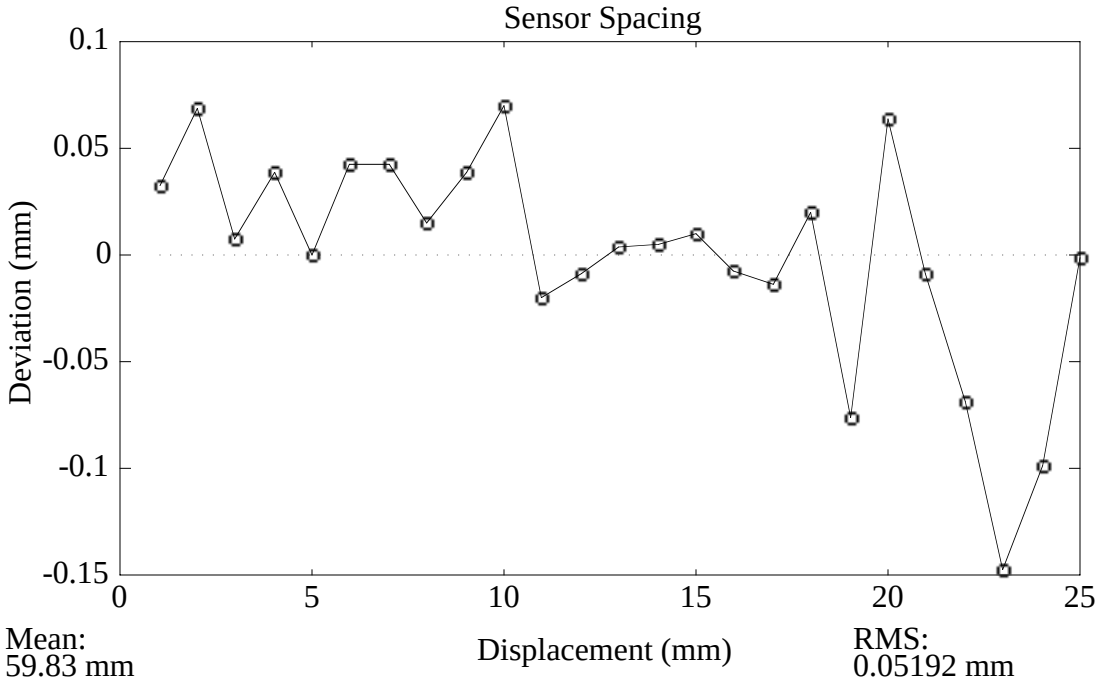

Figure 14: Deviation in reconstructed distance between pickups over local axial displacement

Fig. 14 shows a reconstruction of the distance between pickups as the sensor assembly is scanned (obtained at each point by taking the difference of the β value from one pickup from the linear extrapolation of the other, then vice-versa, and averaging them both). The mean result is nearly 6 mm, which agrees well with the spacing between pickups shown in the mechanical assembly of Fig. 6. More importantly, it is quite constant with displacement, yielding an excursion from average of only 50 μm RMS, vowing for consonance in the data between pickups. The excursions from the mean seem to grow more strenuous near the last points of the test; since the sum data of Fig. 13 also exhibits more activity there, a slight mechanical or electrical disturbance of the system may have occurred or a defect encountered in the wire.

Since the local data from the short-range scan was so promising, the sensor assembly was installed on a single degree-of-freedom coordinate-measuring machine (CMM) capable of translating up to 1.5 meters with an accuracy of better than 200 μm[15].

The setup was analogous to that shown in Fig. 8, except now the wire was 1.7 meters in length (yielding 70 Ω of net resistance), and the sensors could translate nearly to the ends. Data was taken at 5 centimeter intervals.

Fig. 15 shows the raw sensor voltage (now with both pickups sharing a common plot) and Fig. 16 their residuals. The gains on the Techron were balanced better in this test, hence the left and right slopes are in much better agreement. As before, pickup #2 exhibits a stronger response due to its larger area, causing the visible skew in the pickup slopes.

The data looks extremely linear over this wide range, but a peek at the residuals in Fig. 16 expands the deviation from the linear trend, and shows much larger excursions (ranging in RMS from 1-3 mm) than were noted in the short range example of Fig. 10. Again, they appear to have an similar structure, thus are expected to cancel somewhat in the ratio β, which is plotted in Fig. 17 (with linear residuals in Fig. 18). This is indeed happening; Fig. 17 shows a pair of parallel lines from the two pickups tracking each other perfectly over the 1.5 meter range of the test displacement.

The least-squares fit residuals in Fig. 18 expand the departure from linearity, and still indicate a much higher error than in the short-range test of Fig. 12; the RMS deviations are now slightly under a half millimeter, an order of magnitude higher than in the previous example. This is most likely due to mechanical factors; i.e. wire quality, sag, misalignment, and the intrinsic error in the CMM rig. This is supported by the correlated, multi-feature signal detected at both sensors (the residuals of Fig. 18 can be nearly superimposed without discrepancy); the errors are highly structured, and are seen by both pickups.

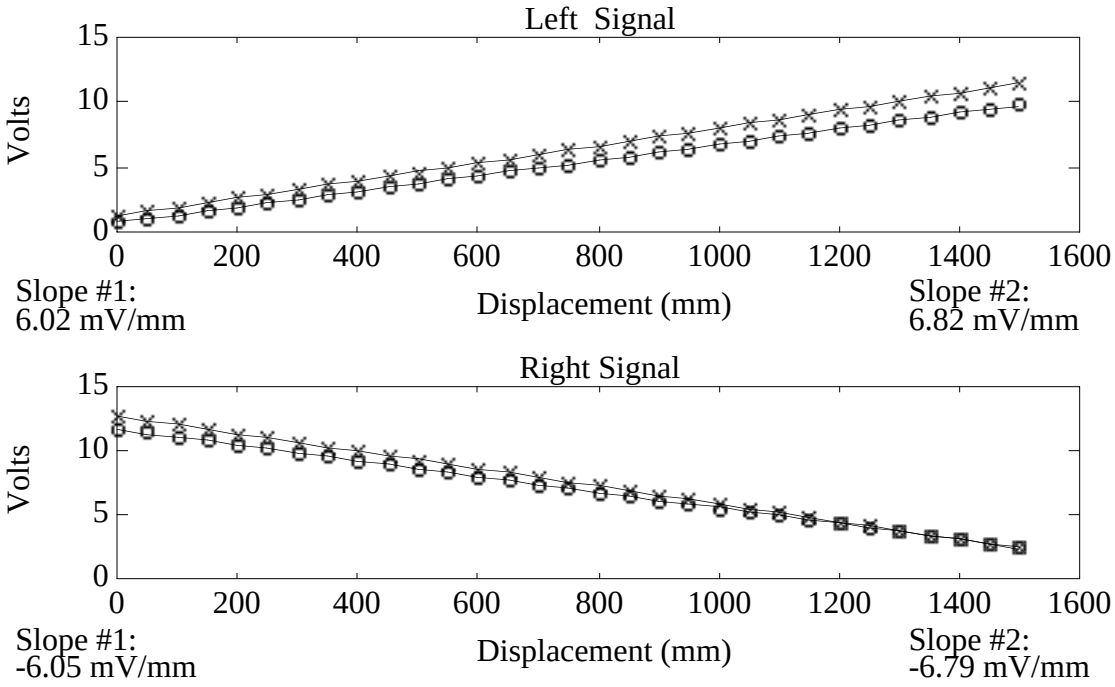

Figure 15: Pickup signals as a function of wide-range axial displacement

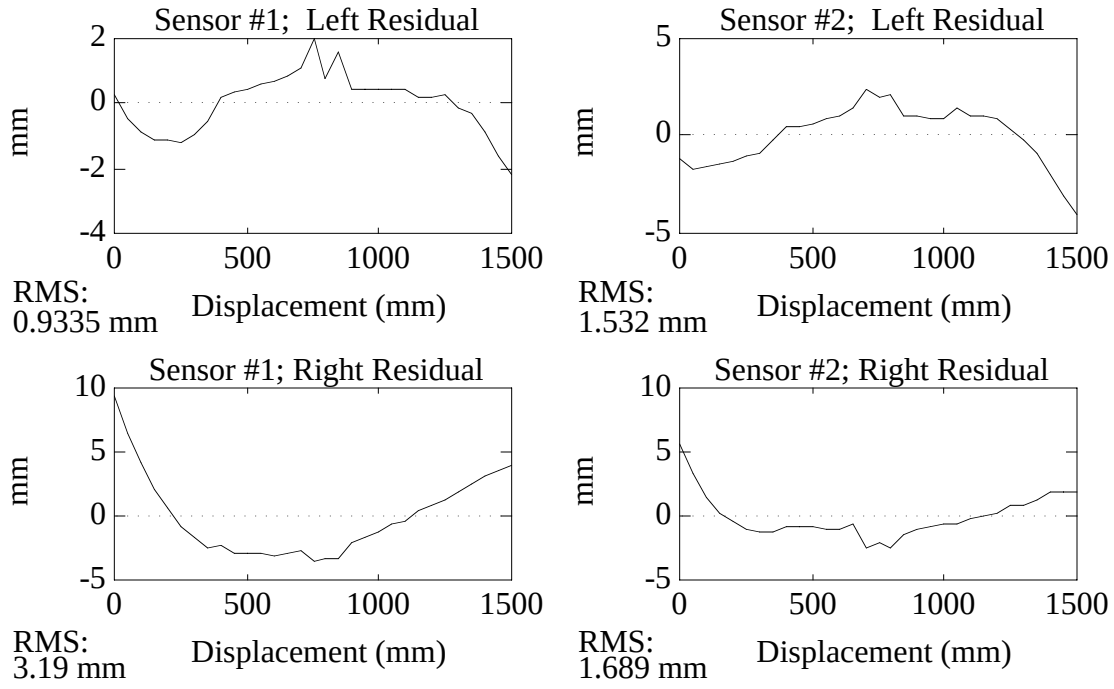

Figure 16: Linear residuals from above pickup signals

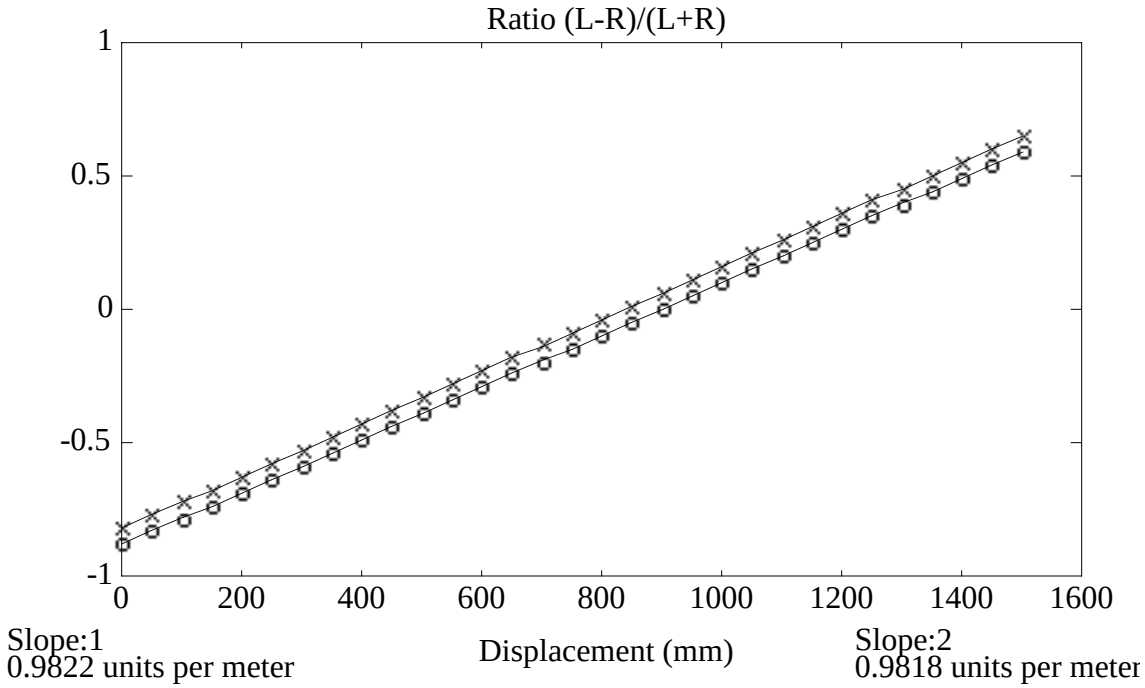

Figure 17: Sum over difference ratio β as a function of wide-range axial displacement

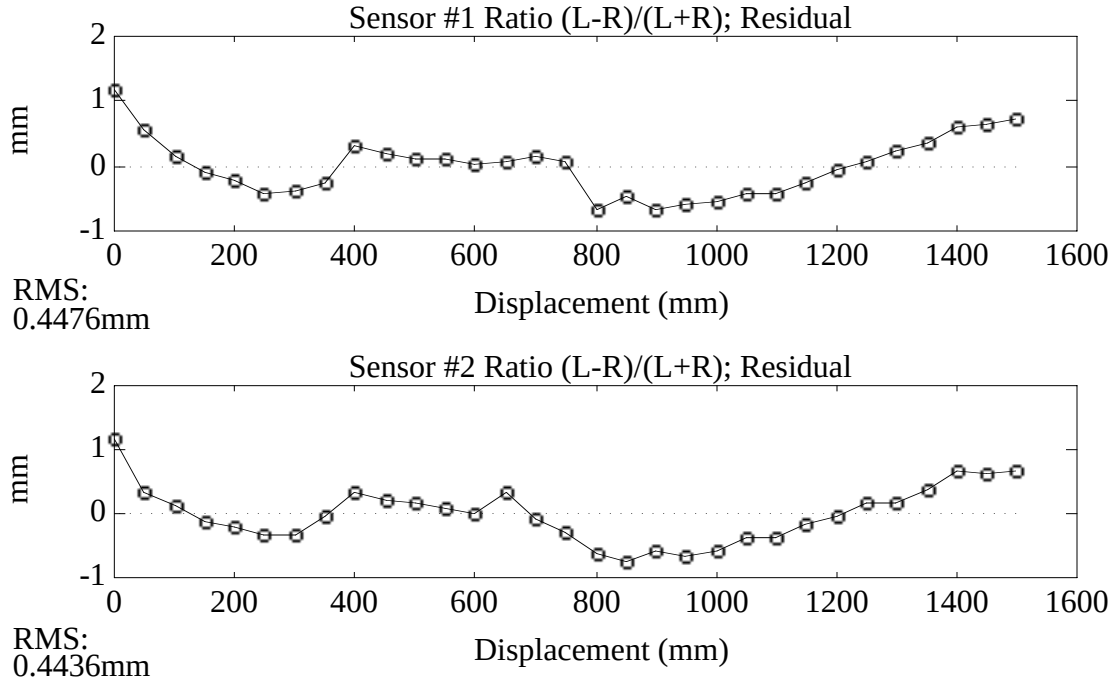

Figure 18: Linear residual of β as a function of wide-range axial displacement

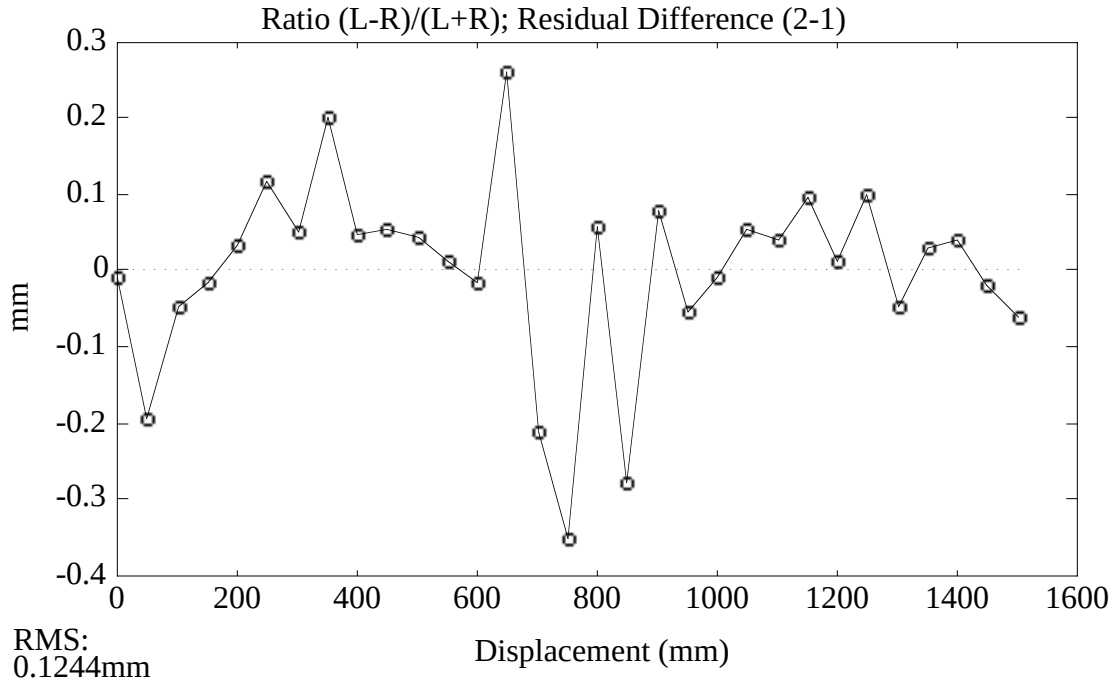

Figure 19: Difference in β residuals between pickups as a function of wide-range axial displacement

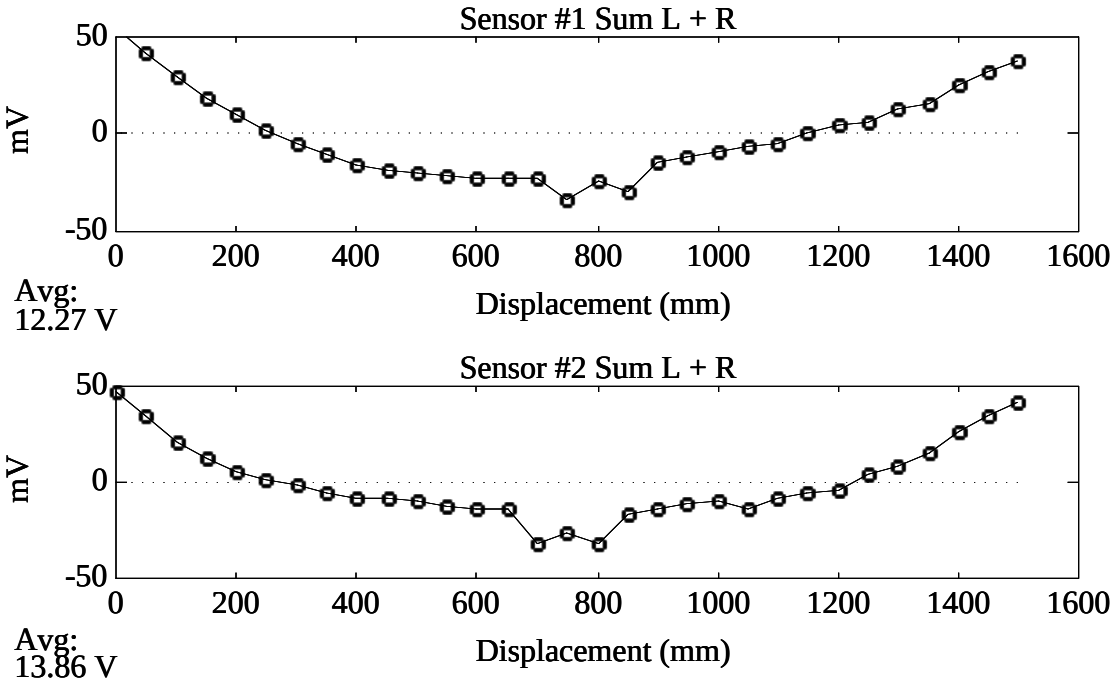

Figure 20: Sum of Left and Right signals from each pickup over wide-range axial displacement

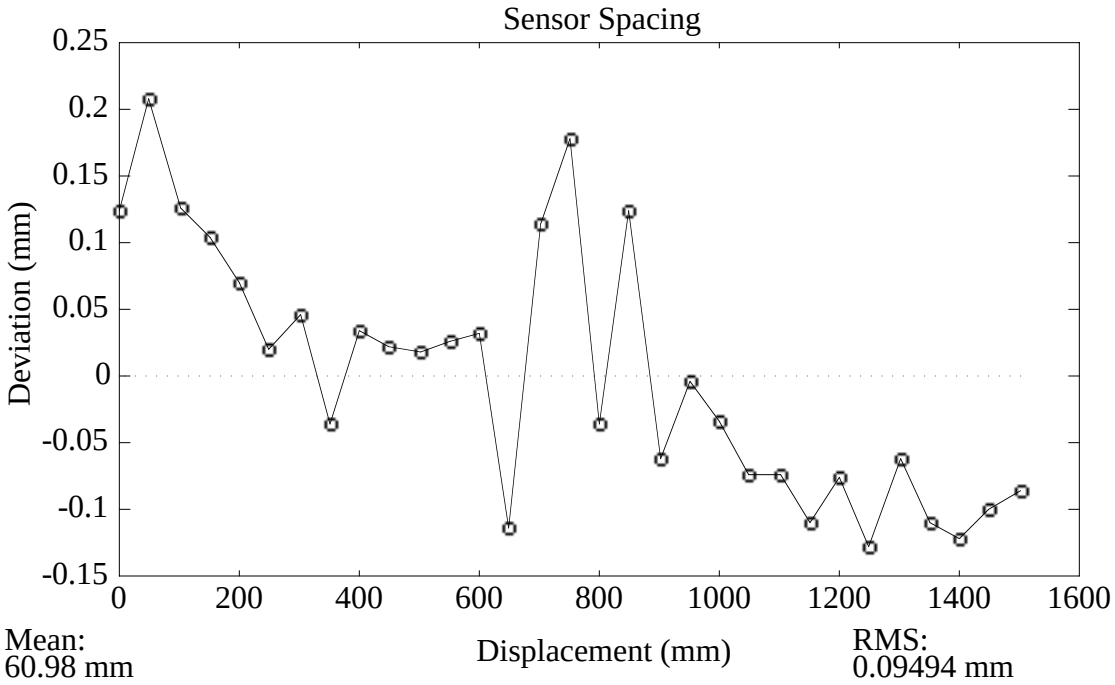

Figure 21: Deviation in reconstructed distance between pickups for wide-range scan

Fig. 19 investigates this further by plotting the difference in residuals between the two pickups. Indeed, the RMS is much smaller now, reaching the vicinity of 125 microns. The feature in the middle of the plot (600-900 mm) is seen to dominate this distribution; upon examining the wire afterwards, a large imperfection was noted at this location; it could easily be felt by running one's finger down the wire, and was evident to the naked eye (rather than a discrete kink, this was a distributed bump that most probably arose in the wire fabrication). This bump threw the local pickup 1/2 tracking off when the sensor assembly was moved past; if it is discounted from Fig. 19, the pickups track one another with an RMS of 75 μm, which is in excellent accord with the resolution gleaned from the short-range data of Fig. 12. The short-range data taken in the previous scan thus appears to describe the level of sensitivity in these measurements as well; when looking over a much longer range, however, mechanical factors and defects in the wire affect the overall accuracy, as outlined in the previous section.

Yet more insight is offered in the sums of left and right signals, plotted in Fig. 20. The bump in the wire is very evident near the center of the scan; it is even clear enough to resolve the 6 cm pickup spacing by observing the shift in feature position between upper and lower plots. The general bow shape of the curve is probably due to wire sag or twist in the measuring device; i.e. the ends of the wire are slightly closer to the pickup walls

(the wire resistance and frequency are too low for significant coupling loss). Looking again at the residual plots (Fig. 18), a form of the generic bow shape appears also to be present (apart from the sharp features made by the bump at 700 mm and the kink at 400 mm, which is probably due to a splice in the CMM support), indicating that such sag has some effect on the axial measurement.

Fig. 21 shows the reconstructed pickup spacing across the scan, and illustrates some relevant effects. The bump at the wire center is again very evident, as is a positive-to-negative trend; the sensor assembly appears to change in length by roughly 200 μm between the beginning and end of the scan. As the assembly is rigid, this is impossible; a more logical inference can be gleaned from the discussion of Fig. 5, which described a pickup rotated and offset relative to the wire. The trend in Fig. 21 is what one would expect from such a situation. If the scan axis is skewed slightly from the wire axis, the offset of pickups from wire will change in proportion to the scan displacement, causing this effect to evolve smoothly with scanner position. Since the scanner setup was rigged quickly "by eye" such misalignments are expected, and Fig. 21 indicates the combined effects of axial misalignment and wire sag. Nonetheless, this effect is relatively small; the RMS deviation across the scan remains under 100 μm, and is still dominated by the bump in the center.

The mean pickup spacing found from the data of Fig. 21 is 6.1 cm; a bit larger than the 6.0 cm spacing seen in the short-range data of Fig. 14, supporting the hypothesis that the sensor assembly was differently rotated in this test.

5) Other Test Results

In addition to the axial scans presented above, other measurements were made to get a further glimpse into system drift and errors arising from wire offsets.

Fig. 22 shows the pickup voltages from a cross-axis scan of the wire, where the pickups were scanned orthogonal to the wire at constant axial distance (the pickups were thus effectively scanned such that the wire moved from one wall of the sensor, through the center, then to the opposite wall). This operation was performed with the setup of Fig. 8; i.e. near the middle of a 3.1 meter length of wire.

A very close similarity can be noted when these profiles are compared to the prediction (Eq. 7, Fig. 4); the device is indeed working as a cylindrical capacitor. Looking more closely at the signals from sensor #1, one notices that the signal level at the +8 mm displacement is significantly higher than that at -8 mm. The situation reverses for sensor #2, where the signal at +8 mm is lower than that at -8 mm. This indicates that the sensor is slightly rotated; i.e. its axis is misaligned with the wire, as depicted in Fig. 5.

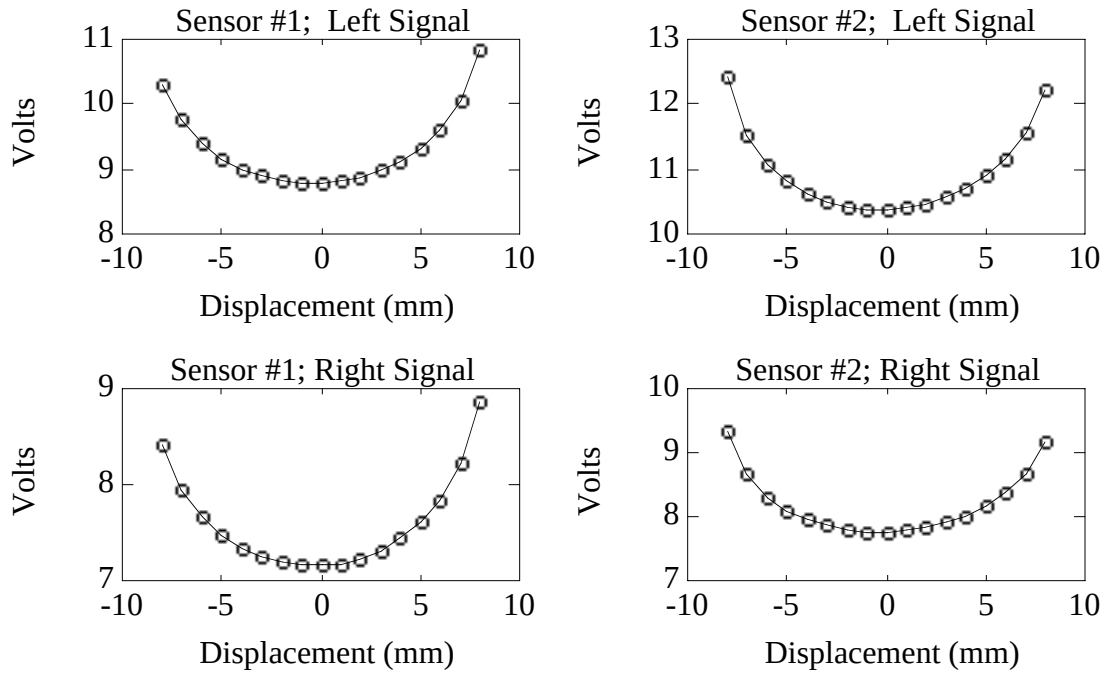

Figure 22: Pickup voltages from cross-axis scan

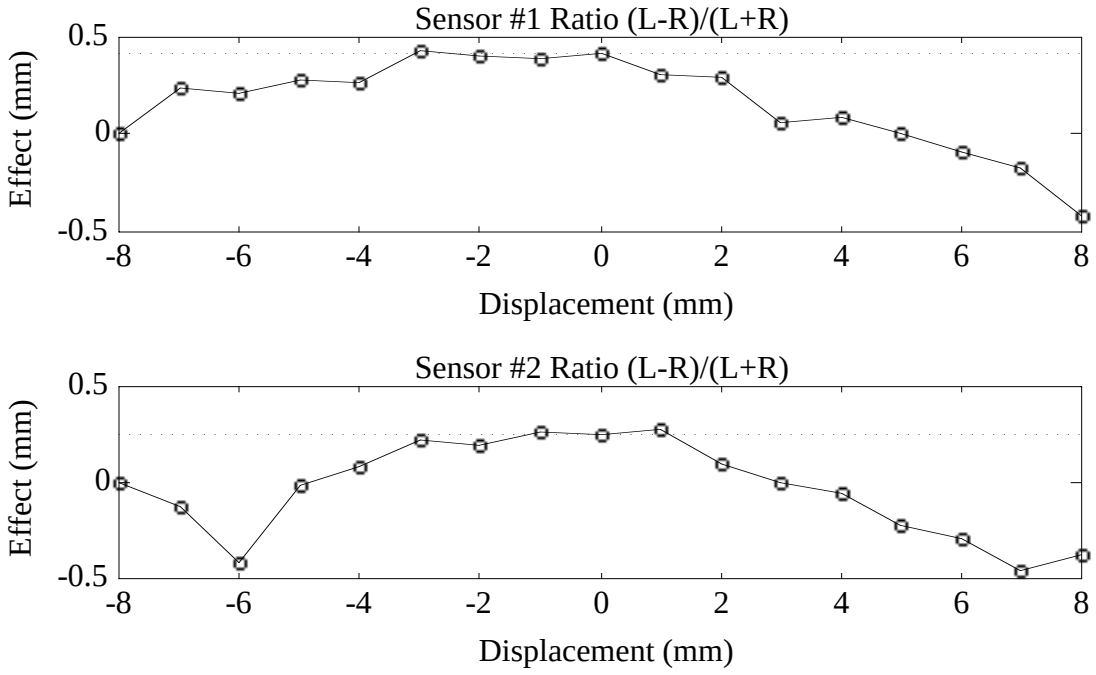

Figure 23: Changes from the ratio β over the cross-axis scan

Fig. 23 shows the axial position shift over the cross-axis scan, as derived from the ratio β, with calibration taken from the lines fit to Fig. 11. A relatively flat region can be noted to span roughly 4 mm near the centers of the pickups (the pickup centers appear to be displaced slightly left of the scan coordinate origin), where displacement has relatively little (i.e. <100 μm) effect on the axial measurement. As the wire is offset further, the effects increase, but generally stay under a millimeter (the small spike in the sensor #2 response at -6 mm may have been due to a mechanical disturbance), despite the fact that the raw sensor signals have increased in strength by roughly 30%.

These results indicate that, even in extreme cases (with the wire at the pickup wall and a modest rotation on the pickup), errors due to effects such as depicted in Fig. 5 are limited to the vicinity of a mm, and are much smaller if the wire is centered within the inner third of the pickup diameter. Again, since these errors are absolute, and do not scale with the length of the wire, they pose no problem for the GEM-like applications discussed in Sec. 1.

Without a computer-based data acquisition system, true measurement drift is difficult to monitor. Ideally, the pickup voltages would be taken with the reference oscillator driving left then right ends of the wire (i.e. the computer would toggle the switch depicted in Fig. 3), and ratio β calculated and tracked. A compromise was pursued, however, by digitizing one of the pickup voltages without toggling the left/right oscillator drive (data was recorded using a Fluke ScopeMeter model 97). While this doesn't provide a good position measurement, it does give an indicator of system drift.

Fig. 24 shows these results taken over a 1 hour interval (the Fluke sampled at roughly 25 Hz) and averaged with a 15 second time constant. The displacements labeled at right were derived from the scale factor fit to a scan associated with this setup (i.e. Fig. 9). The experimental configuration was that of Fig. 8; i.e. the sensor assembly was placed in the midst of a 3.1 meter length of wire.

The top plot (a) was taken when driving the wire with a Tektronix analog oscillator module; one can see a somewhat linear drift in the pickup voltage across the plot. If one scales the data accordingly, this plot indicates a drift of nearly 2 mm!

One must be cautious, however; as stated in Eq. 5, the drive frequency ω appears linearly in the pickup voltage, hence any variation in the frequency of the reference oscillator will propagate through (this variation is removed in the ratio β, which can not be calculated without also measuring relative to the opposite end of the wire).

The drift in the axial measurement may not be nearly so bad, a conjecture that seems supported by the lower plot (b) in Fig. 24. Here a very stable HP 3245a Universal Source was used for the reference oscillator, virtually eliminating the frequency drift and,

as noted in Fig. 24b, likewise restricting the pickup voltage drift to the vicinity of 200 μm, with no trends evident (this oscillator was thus employed to generate all of the test results presented in this report). Again, with a computer-based sampling system, the reference oscillator need only be stable while the left/right-driven data is taken (30 seconds is more than adequate) for the ratio β, thus the stability of the reference is not as important in practice.

Fig. 24b indicates that the mechanical and electronics drift were likewise rather low. Indeed, the latter seemed to be quite stable, but the mechanical configuration employed was less optimal; the wire was strung across a conventional wooden workbench, and measurements could be affected by shifting objects on the benchtop, changes in air conditioning, etc. When collecting data, great care was taken to avoid disturbing the bench; test sessions were also scheduled to avoid rapid thermal cycling from the air conditioning. The data in Fig. 24b and the scan tests presented in the previous section (each of which took over an hour to perform) indicate that the system remained relatively stable, at least over hour-length intervals. This must be tested, however, in a more stable mechanical setting over longer periods of time, with automated readout, and preferably with better quality wire.

One final set of tests were carried out to examine a related topic; that of wire sag. The severity of the sag problem can be debated; by using special composite wires that exhibit very low mass and high strength, wire sag can be appreciably reduced (i.e. a silicon carbide wire[5] can be pulled hard enough to exhibit a sag on the order of 300 μm over a 15 meter length). Sags of this magnitude will have little effect on an axial measurement of the 1.5 mm resolution desired for GEM. For transverse-axial measurements that are needed at the 10 μm level for the sagitta correction[5], however, this sag is much too large to leave unaccounted. It was thus the assumption at GEM that the sag of the wires would be dynamically measured.

The resonant frequency (f_0) of a stretched wire is a function of its tension (and thus its sag). The tension relation may be summarized[16] as:

8) $$f_0^2 = \frac{T}{\pi \rho_m (2Lr)^2}$$

where L is the wire length, r is its radius, T is its tension, and ρ_m is its mass density. With some manipulation, the sag can be substituted for the tension, yielding[16]:

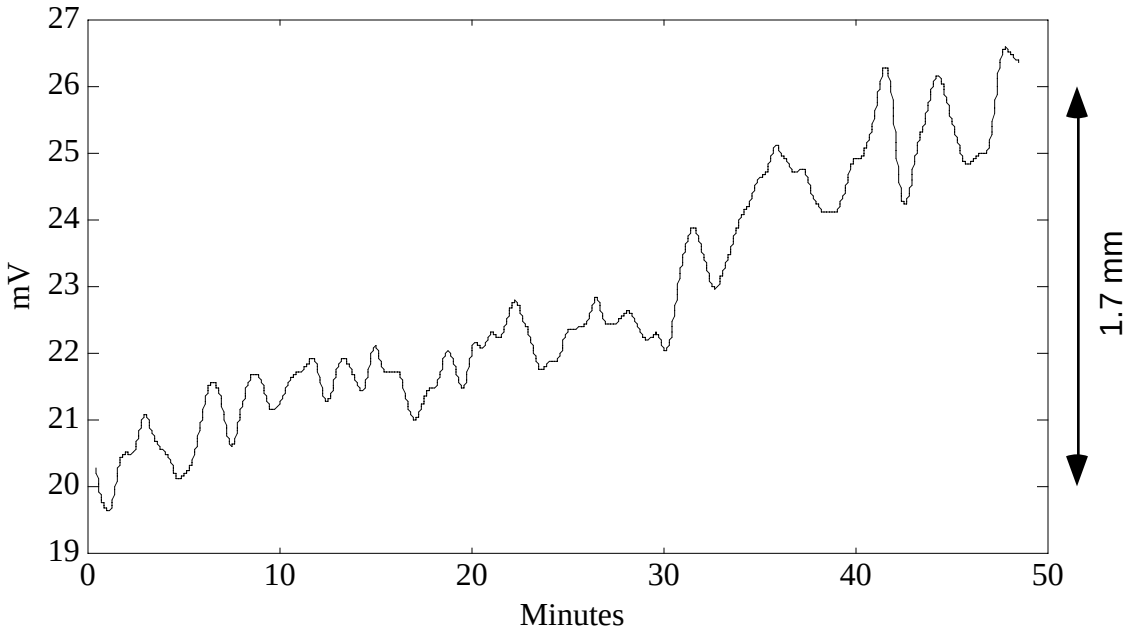

a) Drift using analog Tektronix Oscillator

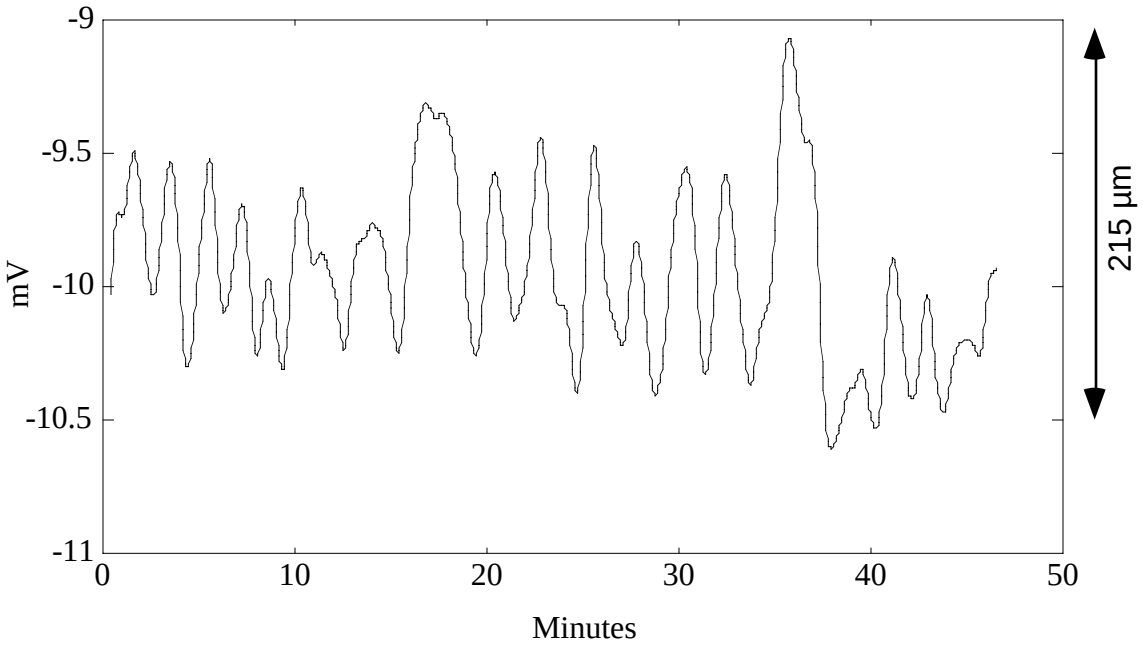

b) Drift using HP3245a Universal Source

Figure 24: Drift in pickup voltages recorded over a 1-hour interval

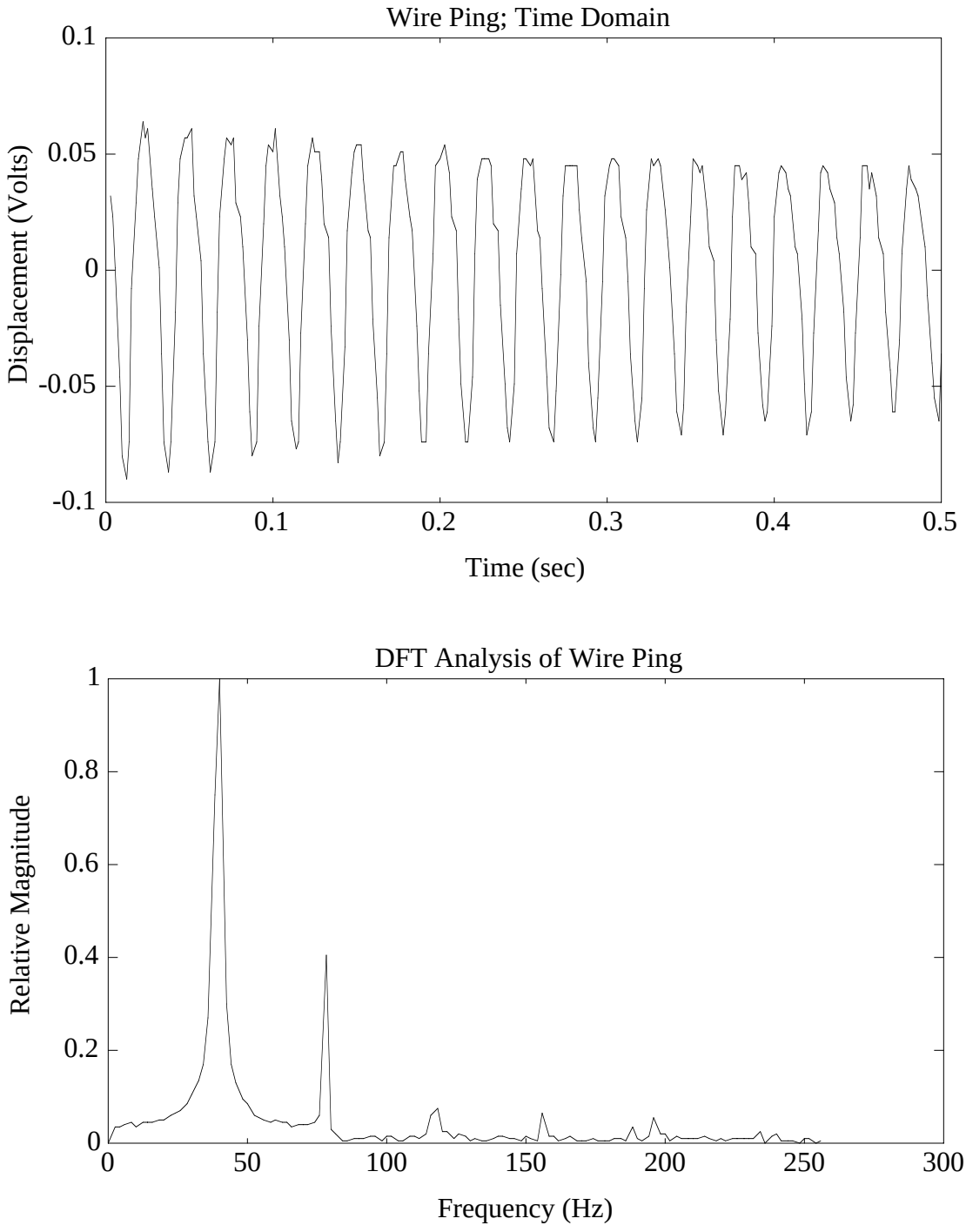

Figure 25: Pickup signal and resulting DFT from small wire pluck

9) $$S = g \frac{\left(\frac{x_L}{x_L + x_R}\right)^2 - \left(\frac{x_L}{x_L + x_R}\right)}{8 f_0^2}$$

where g is gravitational acceleration and x_L, x_R determine the axial position at which wire sag S is measured relative to the left (L) and right (R) ends of the wire, as defined in Fig. 3. By measuring the wire's resonant frequency, one thus can accurately predict the wire sag. In Ref. 15, the sag of a 3.7 meter tungsten wire of ø = 50 μm was predicted to within 5 μm by running a sinusoidal current through a wire in a magnetic field and tuning through its resonant peak.

The synchronous detection electronics used for the pickup strips[6] are very sensitive and rolloff at 300 Hz, thus are well-suited to measure the wire dynamics. By exciting a stretched wire with a small "ping" (using, for example, a piezocrystal at an endpoint support, or exploiting the gradient of the detector's magnetic field and injecting a current pulse as described above), the resulting oscillations may be sampled and the wire resonance determined.

Fig. 25 shows a quick test of this concept. The top plot displays the wire response to such a "ping", created by plucking the wire near its support, and monitoring the demodulated signal coupled into a ministrip placed beneath the wire (the mini-strips were used as opposed to the axial pickup ring because of their sensitivity to transverse displacement; the axial rings show less response to transverse displacement of a centered wire, as plotted in Fig. 4). Data was again taken with the Fluke ScopeMeter; 256 8-bit samples were acquired over a half-second interval. One can clearly note a lightly damped response that appears fairly sinusoidal (the wire was plucked close to its endpoint, exciting higher harmonics); the ministrip is functioning as an excellent "guitar pickup" here.

The lower figure is a Discrete Fourier Transform (DFT) run on this data. Indeed, the fundamental frequency can be determined very precisely due to the highly peaked distribution, hence the wire sag can be accurately calculated via Eq. 9.

6) Conclusions

The axial displacement along a stretched resistive wire has been successfully determined by driving the wire as an AC voltage divider and capacitively coupling the local signal into a set of pickup rings. The technique is remarkably sensitive; in both long-range and short-range scan tests, the local displacement of the sensor assembly could be determined to within 50-100 μm RMS on a wire up to 3.1 meters in length. The full-range axial position was subject to additional error sources (i.e. irregularities in the wire, mechanical misalignment); nonetheless, resolutions of under 500 μm RMS were obtained across a 1.5 meter span of wire. Errors due to axial misalignment and pickup rotation were examined; in normal operation these should stay under a millimeter, and do not scale with the wire length. The system appeared relatively stable (i.e. drift £ 200 μm) over hour-long durations, but should be additionally tested for stability over longer intervals, with longer wires, and under varying temperatures and conditions.

The accuracy and stability of this technique depend heavily upon the properties and uniformity of the wire that is used. By employing a wire of superior mechanical quality and low temperature coefficient, these factors can be adequately constrained, enabling the GEM goal of resolving mm-level displacements on long wires.

The resonant frequency of a 3.1 meter wire was seen to be very well determined by using a pickup strip to measure its displacement when mechanically excited. This provides a straightforward method of calibrating wire sag*in situ*..

7) Acknowlegements

Andrey Korytov, Louie Osborne and Dale Ross at MIT/LNS are earnestly thanked for extending their hospitality and allowing me to run these tests in their laboratory. In addition, Dale's assistance in setting up was highly appreciated. Thanks also to George Brandenburg at Harvard for lending me the spool of uncoated tungsten wire, and to Mike Harris of SSC/CERN for arranging the GEM close-out activity that made this document possible. Neil Gershenfeld at the MIT Media Laboratory is especially acknowledged for lending me the HP instruments used in these tests, along with our many discussions on cello bow position sensing[17], which led to the stretched-wire readout electronics. Finally, this effort benefited significantly from collaboration with my muon colleagues at GEM, namely Gena Mitselmakher, Vinnie Polychronakos, Frank Taylor, Scott Whitaker, and Craig Wuest.

References

[1] “GEM Technical Design Report,” Chapter 4, GEM-TN-93-262.

[2] Paradiso, J., "Some Alignment Concepts for the GEM Muon Array," GEM-TN-92-124, June, 1992.

[3] Paradiso, J., Goodwin, D., "Wide-Range Precision Alignment For The Gem Muon System", Proc. of the Third International Workshop on Accelerator Alignment, Annecy, France, Sept. 28 - Oct. 1, 1993.

[4] Korytov, A., "The Axial + Projective Alignment for Muon Chambers," GEM TN-93-302, March, 1993.

[5] Korytov, A., Osborne, L., Paradiso, J., Rosenson, L. and Taylor, F., "Multi-Point Wide-Range Precision Alignment Technique for the GEM Detector" Nuclear Instruments and Methods in Physics Research, A343, pp. 428-434, 1994.

[6] Paradiso, J., "Synchronous Proximity Detection for Stretched-Wire Alignment Systems" GEM-TN-93-447, August, 1993.

[7] Paradiso, J., "Analysis of an Alignment Scheme for the GEM Muon Barrel," GEM-TN-92-150, October, 1992.

[8] Jones, M., Applied Geodesy Group, SSC Laboratory, personal communication.

[9] Mitselmakher, G. and Ostapchuk, A., "New Approach to Muon System Alignment," GEM TN-92-202, October 1992.

[10] Mitselmakher, G. and Ostapchuk, A., "Alignment Requirements for the GEM Muon System", GEM TN-93-333, March, 1993.

[11] Buskens, J., et. al., "Small High-Pressure Wire Chambers for the Measurement of $p\bar{p}$ Elastic Scattering at the CERN Collider", Nuclear Instruments and Methods, 207, pp. 365-378, 1983.

[12] Reference Data for Radio Engineers (ITT), Fourth Edition, Stratford Press, New York, 1956.

[13] American Institute of Physics Handbook, McGraw-Hill, 1972.

[14] MATLAB, version 3.5, The Math Works, Inc., Cochituate Place, 24 Prime Parkway, Natick, MA. 01760.

[15] Ross, D., MIT/LNS, personal communication.

[16] Ahlen, S., et. al., "Wire Positioning Accuracy Based on Knowledge of Wire Tension", GEM TN-92-74, Feb., 1992.

[17] Gershenfeld, N., "Sensors for Real-Time Cello Analysis and Interpretation", Proc. of the ICMC, Montreal, Canada, 1991.